NANO LETTERS

pubs.acs.org/NanoLett

Letter

Single-atom Catalytic Materials for Lean-electrolyte Ultrastable Lithium–Sulfur Batteries

Chao Lu, Yan Chen, Yuan Yang, and Xi Chen*

Cite This: *Nano Lett.* 2020, 20, 5522–5530

Read Online

ACCESS | Metrics & More | Article Recommendations | Supporting Information

ABSTRACT: Lithium–sulfur batteries with high energy capacity are promising candidates for advanced energy storage. However, their applications are impeded by shuttling of soluble polysulfides and sluggish conversion kinetics with inferior rate performance and short cycling life. Here, single-atom materials are designed to accelerate polysulfide conversion for Li–S batteries. Nitrogen sites in the structure not only anchor polysulfides to alleviate the shuttle effect but also enable high loading of single-atom irons. Density functional theory calculations indicate that single-atom sites reduce the energy barrier of electrochemical reactions and thus improve the rate and cycling performances of batteries. The coin battery shows impressive energy storage properties, including a high reversible capacity of 1379 mAh g^{-1} at 0.1 C and a high rate capacity of 704 mAh g^{-1} at 5 C. The ratio of electrolyte dosage/energy density is as low as 5.5 g Ah^{1-}. It exhibits excellent cycling performance with a capacity retention of 90% even after 200 cycles at 0.2 C.

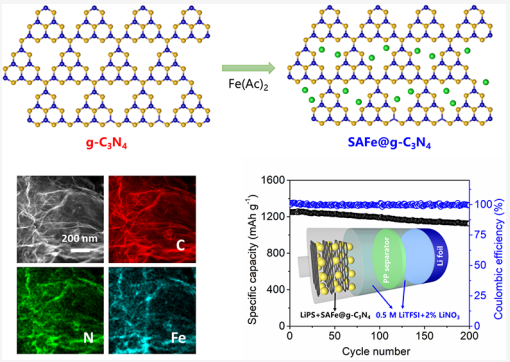

KEYWORDS: *Single-atom materials, Lithium–sulfur batteries, Fast polysulfide kinetics, Lean-electrolyte, Long cyclic life*

Lithium–sulfur (Li–S) batteries are considered promising candidates for advanced energy storage systems owning to the high theoretical energy capacity of 1675 mAh g^{-1} and abundant storage of sulfur element on earth.[1−3] The lithium and sulfur chemistry is capable of exerting multi-electron electrochemical processes to give considerably higher energy densities than commercially available lithium-ion batteries based on insertion-type materials.[4,5] However, commercialization of Li–S batteries is impeded by several scientific challenges, which are mainly caused by sluggish electrochemical conversion kinetics and polysulfide shuttle effects in battery chemistry.[6,7] The sluggish conversion kinetics will deteriorate reversible specific capacities and rate performances of batteries, which makes the fast charge–discharge function impossible.[8,9] On the other hand, polysulfide shuttle effects in Li–S batteries caused by desolvation of polysulfide in ether solvents will seriously lead to loss of sulfur materials and thus result in irreversible specific capacity and short cycling life.[10,11] In addition, the high theoretical energy density of Li–S batteries cannot be fully expressed in practical devices because of the low mass loading of sulfur.[12,13] The limited mass loading is attributed to the insulating nature of sulfur and the tendency of sulfur to agglomerate in the cathode support materials.[14,15] In order to pave the way to practical application of Li–S batteries, a highly active cathode material with high sulfur loading is imperative to address these issues in conversion chemistry.

Single-atom materials have recently attracted enormous attentions for electrocatalytic processes since they maximize the atom utilization with highly active sites, tunable electronic environments, improved chemical stability, and excellent reversibility in contrast to conventional catalytic materials.[16,17] Several examples of single-atom materials for metal–air batteries and fuel cells have been demonstrated in past years with enhanced performance.[18,19] Single-atom materials are considered promising candidates for accelerating electrochemical conversion kinetics of Li–S batteries because the individual catalytic sites with unsaturated metal coordination are believed to facilitate electron transfer and redox reactions in batteries. However, the weight percentage of single-atom sites in the host remained at a relatively low level (less than 3 wt %), since the single atoms are easy to aggregate under high weight percentage.[20,21] It is possible to achieve high mass loading of single atoms by searching for high-polarity support materials through enhancing their coordination interactions.[22] Therefore, the development of high-loading single-atom cathode materials with high catalytic activity is an effective strategy to promote polysulfide conversion chemistry for practical applications of Li–S batteries with high energy density and superior rate capability.

Received: May 21, 2020
Revised: June 23, 2020
Published: June 24, 2020

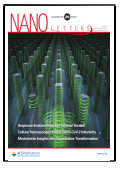

https://dx.doi.org/10.1021/acs.nanolett.0c02167
Nano Lett. 2020, 20, 5522–5530

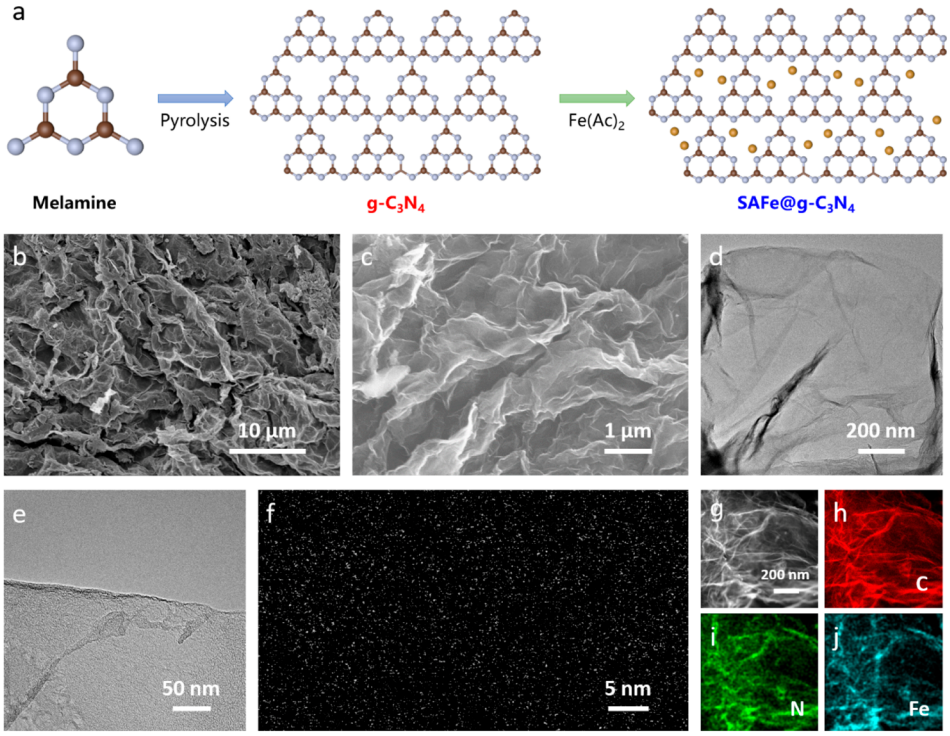

Figure 1. Synthesis and morphology characterization of SAFe@g-C_3N_4 material. (a) Schematic illusion of synthesis procedures. (b, c) SEM images of SAFe@g-C_3N_4 material under different magnifications. (d, e) TEM images of SAFe@g-C_3N_4 material under different magnifications. (f) HAADF-STEM image of SAFe@g-C_3N_4 material showing single iron atoms. (g–j) EDX mappings of carbon, nitrogen, and iron element in SAFe@g-C_3N_4 material, respectively.

In this work, a high-loading single-atom material (SAFe@g-C_3N_4) with superior catalytic activity is put forward for boosting electrochemical conversion kinetics for Li–S batteries. The g-C_3N_4 material is selected as a support for single-atom loading because of numerous nitrogen sites in the structure with strong coordination. This coordination effect makes high loading of single atoms possible, and we achieve as high as 8.5 wt % in the SAFe@g-C_3N_4 materials. In addition, g-C_3N_4 material also effectively suppresses the shuttle effect of polysulfide in the battery, which reduces sulfur loss in charge–discharge processes and has been verified by ultraviolet–visible spectra analysis in the experiments. Density functional theory calculations are utilized to verify the activity of SAFe@g-C_3N_4 in battery conversion kinetics, and the results display that the energy barrier concerning polysulfide conversion is reduced significantly due to single-atom catalytic effects. Moreover, sulfur loading in cathode achieves as high as 2.3 mg cm^{-2} by dispersion of Li_2S_8 catholyte onto SAFe@g-C_3N_4 materials. The high sulfur loading is realized in the cathode because of the high adsorption of sulfur species on g-C_3N_4 and fast electrochemical conversion kinetics of single atoms. Consequently, the SAFe@g-C_3N_4 based Li–S coin battery displays a high reversible specific capacity of 1379 mAh g^{-1} at a current rate of 0.1 C, which approaches the theoretical capacity. It exhibits good rate performances with wide current densities and still delivers high specific capacity of 704 mAh g^{-1} at 5 C. It is worth mentioning that this device presents excellent cycling stability with a capacity retention of 90% even after 200 cycles at current rate of 0.2 C, while Li–S cells with pristine g-C_3N_4 and b-Fe@g-C_3N_4 deteriorate seriously under the same condition. The achieved cycling performance is on par with the best reports in previous works based on various cathode materials. The ratio of electrolyte dosage/energy density is evaluated as low as 5.5 g Ah^{1-}, which is critical for practical application of high energy density Li–S batteries. This study highlights the great potential of highly catalytic single-atom materials with high sulfur loading for practical applications of high energy density Li–S batteries.

Since single-atom materials are particularly interesting for accelerating electrochemical conversion kinetics of battery chemistry, single-atom iron@graphitic carbon nitride (SAFe@g-C_3N_4) is designed here for high-performance Li–S batteries. The synthesis procedures of SAFe@g-C_3N_4 are illustrated in Figure 1a, and experimental details are presented in the Supporting Information. Typically, melamine is utilized as the precursor with the high-temperature exfoliation method for synthesizing g-C_3N_4 material. The layer structure of g-C_3N_4 with a high nitrogen doping level promote coordination with single atoms will increase single-atom mass loading without serious aggregation. Moreover, nitrogen atoms with strong polarity act as an adsorbent for polysulfide and thus suppress the shuttle effect in Li–S batteries, which will avoid sulfur loss during cycling and improve the utilization ratio of sulfur species. Subsequently, single iron atoms are introduced into g-C_3N_4 structure utilizing $Fe(Ac)_2$ (ferrous acetate) as a precursor with further high-temperature reduction step. Optical images of g-C_3N_4 and SAFe@g-C_3N_4 materials with yellow and black colors are presented for comparison in Figure S1. Chemical structure of SAFe@g-C_3N_4 material in the schematic illustrates that single iron atoms anchor with nitrogen sites in g-C_3N_4 structure through coordination effects.

Scanning electron microscopy (SEM) images in Figure 1b and c show the layered structure of SAFe@g-C_3N_4 material at different magnifications, and the structure of g-C_3N_4 was

https://dx.doi.org/10.1021/acs.nanolett.0c02167
Nano Lett. 2020, 20, 5522–5530

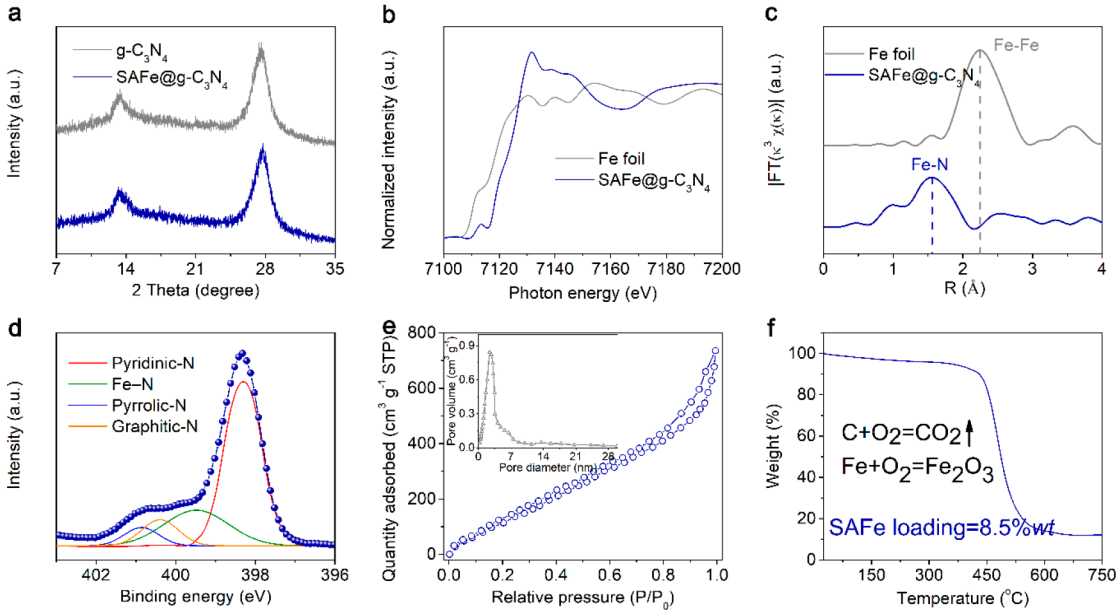

Figure 2. Chemical structure analysis of SAFe@g-C_3N_4 material. (a) XRD patterns of g-C_3N_4 and SAFe@g-C_3N_4 materials. (b) Fe K-edge XANES spectra of Fe foil and SAFe@g-C_3N_4 material. (c) Fourier transformed curves of the Fe K-edge EXAFS spectra of Fe foil and SAFe@g-C_3N_4 material. (d) Deconvoluted N 1s XPS spectra of SAFe@g-C_3N_4 material. (e) N_2 adsorption/desorption isotherm of SAFe@g-C_3N_4 material. Inset shows the pore size distribution. (f) TGA curve of SAFe@g-C_3N_4 material under air atmosphere. Single iron atom mass loading is achieved at 8.50 wt % in the material.

retained well within the following reduction process. Transmission electron microscopy (TEM) images in Figure 1d and e clearly present its thin planar structure, and the morphology of g-C_3N_4 material is presented in Figure S2 for comparison. In order to clarify distribution of iron atoms in the material, the high-angle annular dark-filed scanning TEM (HAADF-STEM) was applied to record single iron atoms under atomic resolution. As shown in Figure 1f, it is clearly observed that numerous bright dots exist with a uniform distribution of size without significant aggregations, which are attributed to single iron atoms in the sample. From the energy dispersive X-ray (EDX) spectrometry elemental mappings in Figure 1g–j, it can be concluded that carbon (C), nitrogen (N), and iron (Fe) atoms are homogeneously and uniformly distributed in the layered structure of SAFe@g-C_3N_4 material. The atomic ratio of elements from the EDX result is provided in Table S1. As the quantitative analysis of atomic ratio with EDX method is not very accurate because of the low detection limit and existing interference factors, the iron content in Table S1 is lower than the result from thermogravimetric analysis, which is just for qualitative analysis.

To verify the microstructure of the SAFe@g-C_3N_4 material, structural characterizations with X-ray diffraction (XRD), X-ray absorption fine structure (XAFS) spectroscopy, X-ray photoelectron spectroscopy (XPS), nitrogen adsorption/desorption isotherm analysis, and thermogravimetric analysis (TGA) were conducted. The XRD pattern of the SAFe@g-C_3N_4 material in Figure 2a shows two typical peaks at 13.1° and 27.5° for g-C_3N_4 support without any crystalline peaks of iron, which indicates no formation of crystallized Fe. As displayed in Figure 2b, the X-ray absorption near-edge structure (XANES) spectrum of SAFe@g-C_3N_4 material, and its first derivative XANES spectrum, is very distinct from that of metallic Fe foil. This means that iron element exists in the form of single atoms in SAFe@g-C_3N_4 material rather than as an aggregation as crystalline iron. Fourier transformed curves of the Fe K-edge EXAFS spectra of Fe foil and SAFe@g-C_3N_4 material are presented in Figure 2c for further verification of the iron state in the material. In contrast to the spectra of Fe foil, no apparent peaks in the range from 2 to 4 Å attributing to Fe–Fe coordination appeared in the spectra of SAFe@g-C_3N_4 material.[23,24] Otherwise, the spectrum of SAFe@g-C_3N_4 has a typical peak at 1.54 Å, which is ascribed to Fe–N coordination in the structure.[25,26]

XPS spectra of SAFe@g-C_3N_4 material have been obtained to address the coordination state of iron (Figure S3), and N 1s XPS spectra (Figure 3e) can be deconvoluted into several peaks. The peaks at 398.3, 399.5, 400.4, and 400.9 are assigned to pyridinic-N, Fe–N, pyrrolic-N, and graphitic-N, respectively.[27–29] Iron element in the material mainly exists in the form of single atoms by coordination with nitrogen atoms in g-C_3N_4 support. The specific surface area of SAFe@g-C_3N_4 material achieved as high as 709 $m^2\ g^{-1}$, and the pore size was distributed around at 2.6 nm (Figure 2e). The high surface with porous structure is beneficial to high loading of sulfur species and facilitates material transportation.[30] A TGA curve was recorded under air atmosphere with a heating rate of 2 °C min^{-1} for clarifying loading of iron atoms (Figure 2f). Carbon and nitrogen elements will disappear because of the reaction with oxygen while iron element will be retained, forming ferric oxide (Fe_2O_3). Mass loading of a single iron atom achieves as high as 8.5 wt %, which is much higher than results from previously reported works.[31–34] The ultraviolet–visible (UV–vis) spectrum of Li_2S_8 catholyte solutions was obtained to demonstrate the ability of SAFe@g-C_3N_4 material on trapping polysulfide (Figure S4). The comparison of Li_2S_8 catholyte solution before and after adsorption of the material indicates excellent affinity to polysulfide.

In order to understand the energy storage capability of SAFe@g-C_3N_4 material in Li–S battery, a coin cell was fabricated based on the material utilizing Li foil and polypropylene (PP) membrane as anode and separator,

https://dx.doi.org/10.1021/acs.nanolett.0c02167
Nano Lett. 2020, 20, 5522–5530

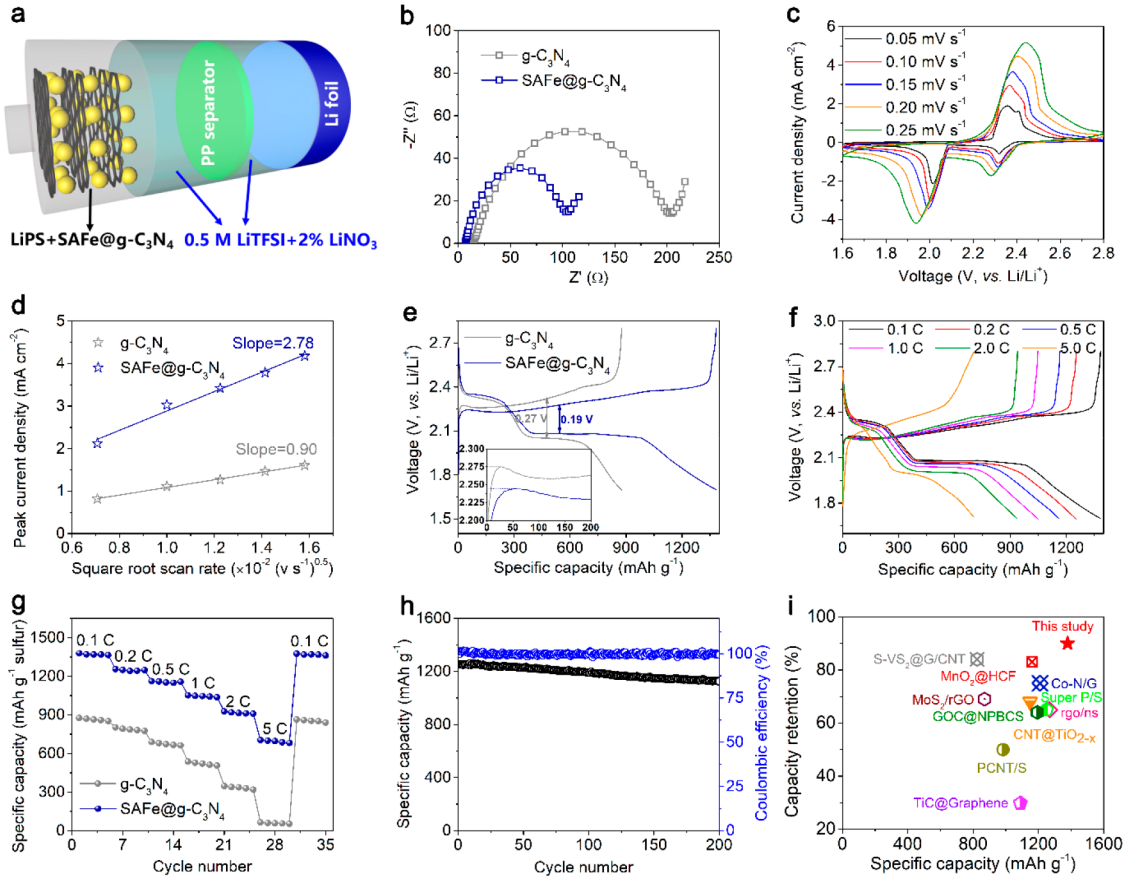

Figure 3. Electrochemical performances of a SAFe@g-C_3N_4-based Li−S battery. (a) Schematic for the structure of battery cell. (b) EIS curves of g-C_3N_4 and SAFe@g-C_3N_4 material-based devices. (c) CV curves of SAFe@g-C_3N_4 material-based device under various scan rates. (d) Plots of the peak currents of the second cathodic process ($Li_2S_x \rightarrow Li_2S_2/Li_2S$) versus square root of scan rates. (e) Galvanostatic charge−discharge curves of the two devices at 0.1 C. Inset shows the potential barrier of the two devices. (f) Voltage−capacity profiles of the SAFe@g-C_3N_4-based device under different rates. (g) Rate performance of the SAFe@g-C_3N_4-based device at rates from 0.1 to 5.0 C. (h) Cycling performance of the SAFe@g-C_3N_4-based device at the rate of 0.2 C for 200 cycles. (i) Comparison of specific capacity and capacity retention of Li−S batteries based on various cathode materials.

respectively. The schematic for battery cell is illustrated in Figure 3a and the detailed assembly procedures are provided in Supporting Information. The Li−S battery with a lower electrolyte to sulfur ratio (E/S) of 3.8 g E/g S, which is essential for practical applications for high sulfur loading cathodes. Lean-electrolyte for Li−S batteries at high capacity is mainly impeded by the kinetic limit of polysulfide in a limited amount of electrolyte. The as-designed SAFe@g-C_3N_4 with high catalytic activity can effectively promote conversion kinetics of polysulfide. The incorporation of single atoms into the cathode greatly reduces the energy barrier of polysulfide conversions, which has been verified by DFT results. The enhanced sulfur electrochemistry will improve utilization of sulfur species and alleviate consumption of electrolyte. Moreover, the good affinity of SAFe@g-C_3N_4 with polysulfide avoids the dissolution and shuttling effects of sulfur species and then reduces the dependence of electrolyte amount. The sulfur loading of the SAFe@g-C_3N_4-based cathode achieves a value of 2.3 mg cm^{-2}, which is much higher than that in previously reported works and is promising for practical applications.[35,36] The mass ratio of the cathode composition has been evaluated (sulfur/SAFe@g-C_3N_4/PVDF/carbon black = 21:8:1:1). Electrochemical impedance spectroscopy (EIS) results of batteries based on g-C_3N_4 and SAFe@g-C_3N_4 materials are presented in Figure 3b. The smaller semicircle diameter in the EIS plot of the SAFe@g-C_3N_4-based device means a smaller charge transfer resistance of the cell, which implies faster charge transfer kinetics in the interface in contrast to that of a g-C_3N_4-based device. On the one hand, distribution of iron atoms in the g-C_3N_4 skeleton improves the electrical conductivity of the material and thus enables faster electron conduction during electrochemical processes. On the other hand, incorporation of iron atoms into the structure will increase the interlayer distance of g-C_3N_4 materials, which can facilitate the ion migration under charge−discharge conditions.

The scan-rate-dependent cyclic voltammetry (CV) curves for the two battery cells are displayed in Figure 3c and Figure S5. The cathodic peak current densities present a linear relationship with the square root of scanning rates in terms of the classical Randles−Sevick equation, and the slope value shows proportional relation with the ion diffusion coefficient.[37,38] Figure 3d shows plots of second cathodic peak currents ($Li_2S_x \rightarrow Li_2S_2/Li_2S$) as a function of the square root of scan rates. It is found that the SAFe@g-C_3N_4-based device displays a higher peak current and slope than those of the g-C_3N_4-based device, which verifies its faster lithium ion diffusion process. Galvanostatic charge−discharge curves of the two devices at a current rate of 0.1 C are compared in

https://dx.doi.org/10.1021/acs.nanolett.0c02167
Nano Lett. 2020, 20, 5522−5530

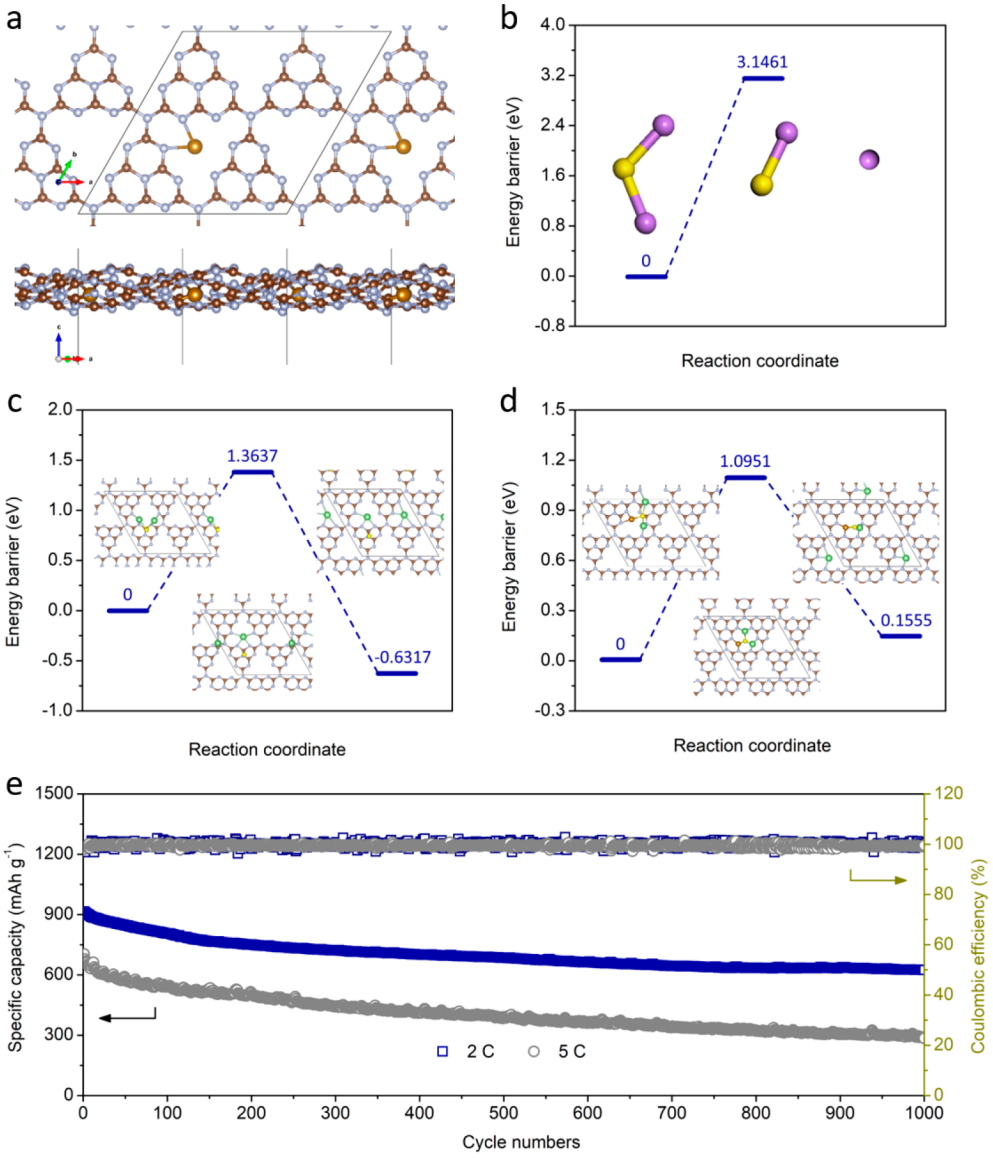

Figure 4. Mechanism analysis and long-term stability evaluation of a SAFe@g-C_3N_4-based Li−S battery. (a) Top and side views of the optimized corrugated configuration of SAFe@g-C_3N_4. Energy profiles of delithiation of (b) pristine Li_2S, (c) Li_2S/g-C_3N_4, and (d) Li_2S/SAFe@g-C_3N_4. Insets in figures show the initial, transition, and final structures. The brown, yellow, green, off-white, and gray balls represent C, S, Li, N, and Fe atoms, respectively. (e) The long-term stability of the device at current rates of 2 and 5 C.

Figure 3e. There exist two typical discharge plateaus at 2.32 and 2.10 V, and two charge plateaus at 2.26 and 2.35 V, which are in good agreement with the electrochemical reactions reflected in the CV results. Compared with g-C_3N_4-based device, the SAFe@g-C_3N_4-based device exhibits a lower voltage polarization of 0.19 V and a higher specific capacity of 1379 mAh g^{-1} at a current rate of 0.1 C. The areal capacity has been evaluated as 3.12 mAh cm^{-2}. The distinct variations of voltage hysteresis and plateau lengths are related to the electrochemical reaction kinetics and the reversibility of sulfur species conversion. The inset in Figure 3e shows the potential barrier of the two devices, and the introduction of single iron atoms significantly reduces the delithiation barrier, indicating faster initial lithium ion kinetics owing to the catalytic effect.

To further testify the enhanced conversion kinetics of the single-atom cathode in batteries, rate performances of the sulfur cathode with g-C_3N_4 and SAFe@g-C_3N_4 have been compared (Figure 3g). The SAFe@g-C_3N_4-based device delivers specific discharge capacities of 1379, 1255, 1162, 1053, 926, and 704 mAh g^{-1} at 0.1, 0.2, 0.5, 1, 2, and 5 C rates, respectively. After the current rate is reduced back to 0.1 C, its specific capacity is recovered to 1368 mAh g^{-1}, which reflects the cell's high reversibility. Benefiting from enhanced reaction kinetics, the electrolyte dosage per energy density achieves a value as as low as 5.5 g A h^{-1}, and the low consumption of electrolyte is essential for practical Li−S batteries to demonstrate the advantage of high-energy density, especially for high sulfur loading cathodes. Notably, voltage plateaus of the SAFe@g-C_3N_4-based cell are clear while those of the g-C_3N_4-based one become indiscernible in Figure S6. The voltage hysteresis of the g-C_3N_4 cell is also much larger than that of the SAFe@g-C_3N_4 cell (0.60 mV vs 0.35 mV in Figure S7). These phenomena illustrate that the single-atom materials play critical roles in enhancing the kinetics of Li−S batteries.

The SAFe@g-C_3N_4 cell also shows an excellent cycling performance (Figure 3h). The high initial specific capacity is

https://dx.doi.org/10.1021/acs.nanolett.0c02167
Nano Lett. 2020, 20, 5522−5530

1255 mA h g^{-1} and maintains at 1129 mA h g^{-1} after 200 cycles at a current rate of 0.2 C. The Coulombic efficiency is 99.5%. The voltage profiles of SAFe@g-C_3N_4-based cells are also stable upon cycling, indicating little voltage degradation (Figure S8). This cycling performance significantly not only exceeds that of the g-C_3N_4-based device in Figure S9 but also outperforms various notable results in the literature.[39−42] The cyclic voltage−capacity profiles in Figure S10 imply the serious capacity deterioration and large voltage polarization after 200 cycles at 0.2 C. The g-C_3N_4 material loaded with bulk Fe (named as b-Fe@g-C_3N_4) has been synthesized as a control sample, and the TEM image in Figure S11 verifies the bulk structure of the Fe component. The cycling profile of the b-Fe@g-C_3N_4-based device in Figure S12 clearly clarifies that its electrochemical performance is slightly better than that of a pristine g-C_3N_4-based device but is worse than that of a SAFe@g-C_3N_4-based device. Single-atom materials with much higher catalytic properties significantly reduce the energy barrier of electrochemical reactions.

A comparison of the specific capacity and capacity retention of Li−S batteries based on various cathode materials is presented in Figure 3i. It is found that SAFe@g-C_3N_4 cathode material can compete with most cathode materials reported previously, such as MnO_2/rGO, MoS_2/rGO, PCNT-S, Co−N/G, TiC@G, S-VS_2@G/CNT, GOC@NPBCS, and so on.[43−52] A comprehensive performance comparison of existing cathode materials is provided in Table S2. The electrolyte dosage can be controlled to a lower level, but the device still delivers a high capacity with ultrastable life. The key advantage of SAFe@g-C_3N_4 materials lies in the role of facilitating the efficiency of material and energy exchange and in improving sulfur utilization. Existing cathodes in Li−S batteries are mainly based on two strategies to immobilize sulfur species and present shuttle effects. One is to introduce heteroatoms with strong polarity into the cathode, including nitrogen, boron, and sulfur atoms.[53−55] The polar heteroatoms in the structure produce strong interactions with sulfur species and thus alleviate their dissolution into the electrolyte. The other strategy is to design hierarchical structures in the cathode, such as tube-in-tube structures and yolk−shell heterostructures.[56,57] Hierarchical structures with confinement effects can immobilize sulfur species and prevent dissolution. The SAFe@g-C_3N_4 material has some differences with the cathode materials mentioned above. The numerous nitrogen atoms existing intrinsically in the g-C_3N_4 structure function as an adsorbent for polysulfides and prevent dissolution and shuttle effects. In addition, the highly active single atoms facilitate kinetics of polysulfide conversion, which avoids drawback effects of immobilized polysulfide. The immobilization−conversion mechanism is different from previous works, and its preparation does not involve complicated hierarchical structure design or the heteroatom doping process. With the rapid development of the smart electronics market, it is urgent to develop high-rate batteries with long cycling life for durable and superfast charging energy supply. A single-atom catalytic cathode with boosting conversion kinetics provides great potential for the market requirements.

In order to clarify the mechanism for improved reaction kinetics of the charge/discharge of a SAFe@g-C_3N_4-based Li−S battery, first-principles calculations based on density functional theory (DFT) have been performed, where we investigated the energy barriers of the delithiation process of different materials. Figure 4a presents top and side views of the optimized corrugated configuration of SAFe@g-C_3N_4, and Fe atoms are stabilized by N atoms in the g-C_3N_4 structure. The lithium evolution processes in a Li−S battery mainly consists of a Li−S bond breaking and leaving of the lithium ion.[58] As shown in Figure 4b, pristine Li_2S is hard to delithiate because of the high energy barrier of 3.1461 eV, and incorporation of catalytically active components into the cathode is critical to accelerating polysulfide conversions. In this work, g-C_3N_4 and SAFe@g-C_3N_4 materials have been introduced into cathodes with the purpose of reducing the energy barrier of the delithiation process and then facilitating the conversion kinetics of polysulfide species.

From the energy profiles in Figure 4c and 4d, it is clearly found that the two materials with active sites both accelerate the Li_2S transformation process and improve sulfur utilization in Li−S batteries. Notably, the highly active single-atom Fe sites in the g-C_3N_4 structure dramatically decrease the energy barrier of delithiation from 3.1461 to 1.0951 eV, which greatly promotes reversible electrochemical conversion reactions during the long-term cycling process. The long-term stability of a SAFe@g-C_3N_4-based device was tested at high current rates of 2 and 5 C in Figure 4e. The initial specific capacities are 915 and 704 mAh g^{-1} at 2 and 5 C, of which 624 and 285 mAh g^{-1} are still available at the end of 1000 cycles (68.2% and 40.5% capacity retention), respectively. Further, the device shows a high Coulombic efficiency close to 100% during the long-term cycling. The as-shown stability performances outperform those of previous works based on other catalytic materials.[49,59−62] DFT calculation details are presented in the Supporting Information (from Figure S13 to S16). These results verify the significance of single-atom sites in boosting electrochemical performances of Li−S batteries and will shed light on the design of active materials for other advanced battery systems.

In summary, a highly active single-atom material (SAFe@g-C_3N_4) was designed for high-performance cathodes in Li−S batteries. Numerous nitrogen sites in a g-C_3N_4 support not only anchor more single-atom sites with a high loading of 8.5 wt % but also stabilize polysulfide to alleviate the shuttle effect during charge−discharge processes. DFT calculations verify that the atomically dispersed single-atom sites in the cathode greatly reduce the energy barriers of electrochemical conversions and made fabrication of high rate and stable Li−S batteries with practical sulfur loading possible. The SAFe@g-C_3N_4-based Li−S coin batteries with a sulfur loading of 2.3 mg cm^{-2} present impressive energy storage performances with a high reversible capacity of 1379 mAh g^{-1} at 0.1 C. The devices also display high rate capability from wide current densities from 0.1 to 5 C and give a much higher specific capacity than pure g-C_3N_4 material-based batteries, which indicates the critical role of highly active single-atom catalytic materials in battery chemistry. It is worth mentioning that the SAFe@g-C_3N_4-based device shows impressive cycling stability with a capacity retention of 90% even after 200 cycles, which can compete with most mainstream cathode materials for Li−S batteries. The improved reaction kinetics caused by single atoms allow for low consumption of electrolyte (E/S = 3.8 g E/g S), and the mass ratio of electrolyte dosage per energy density achieve a value as low as 5.5 g A h^{-1}, displaying enormous potential for practical applications. This study opens a new route to practical applications of high energy density Li−S batteries with excellent rate capability through a material

https://dx.doi.org/10.1021/acs.nanolett.0c02167
Nano Lett. 2020, 20, 5522−5530

engineering strategy for accelerating material and energy exchange kinetics.

■ ASSOCIATED CONTENT

Supporting Information

The Supporting Information is available free of charge at https://pubs.acs.org/doi/10.1021/acs.nanolett.0c02167.

Experimental methods, including details on the materials, synthesis of g-C_3N_4 material, synthesis of SAFe@g-C_3N_4 material, fabrication of Li−S coin battery, DFT calculations, computational details, material characterization, electrochemical measurements, and additional figures and tables (PDF)

■ AUTHOR INFORMATION

Corresponding Author

Xi Chen − *Department of Earth and Environmental Engineering, Columbia University, New York, New York 10027, United States;* orcid.org/0000-0002-1263-1024; Email: xichen@columbia.edu

Authors

Chao Lu − *Department of Earth and Environmental Engineering, Columbia University, New York, New York 10027, United States;* orcid.org/0000-0003-4747-4943

Yan Chen − *Department of Earth and Environmental Engineering, Columbia University, New York, New York 10027, United States*

Yuan Yang − *Department of Applied Physics and Applied Mathematics, Columbia University, New York, New York 10027, United States*

Complete contact information is available at: https://pubs.acs.org/10.1021/acs.nanolett.0c02167

Notes

The authors declare no competing financial interest.

■ ACKNOWLEDGMENTS

This work was supported by the Earth Engineering Center, Center for Advanced Materials for Energy and Environment at Columbia University, and by startup funding from Columbia University.

■ REFERENCES

(1) Seh, Z. W.; Sun, Y.; Zhang, Q.; Cui, Y. Designing high-energy lithium-sulfur batteries. *Chem. Soc. Rev.* **2016**, *45*, 5605−5634.

(2) Yang, Y.; Zheng, G.; Cui, Y. A membrane-free lithium/polysulfide semi-liquid battery for large-scale energy storage. *Energy Environ. Sci.* **2013**, *6*, 1552.

(3) Zhou, G.; Zhao, S.; Wang, T.; Yang, S.-Z.; Johannessen, B.; Chen, H.; Liu, C.; Ye, Y.; Wu, Y.; Peng, Y.; Liu, C.; Jiang, S. P.; Zhang, Q.; Cui, Y. Theoretical Calculation Guided Design of Single-Atom Catalysts toward Fast Kinetic and Long-Life Li−S Batteries. *Nano Lett.* **2020**, *20*, 1252−1261.

(4) Peng, H.-J.; Huang, J.-Q.; Cheng, X.-B.; Zhang, Q. Review on High-Loading and High-Energy Lithium−Sulfur Batteries. *Adv. Energy Mater.* **2017**, *7*, 1700260.

(5) Ji, X.; Lee, K. T.; Nazar, L. F. A highly ordered nanostructured carbon-sulphur cathode for lithium-sulphur batteries. *Nat. Mater.* **2009**, *8*, 500−506.

(6) Manthiram, A.; Fu, Y.; Su, Y.-S. Challenges and prospects of lithium−sulfur batteries. *Acc. Chem. Res.* **2013**, *46*, 1125−1134.

(7) Manthiram, A.; Fu, Y.; Chung, S. H.; Zu, C.; Su, Y. S. Rechargeable lithium-sulfur batteries. *Chem. Rev.* **2014**, *114*, 11751−11787.

(8) Larcher, D.; Tarascon, J. M. Towards greener and more sustainable batteries for electrical energy storage. *Nat. Chem.* **2015**, *7*, 19−29.

(9) Lu, C.; Fang, R.; Chen, X. Single-Atom Catalytic Materials for Advanced Battery Systems. *Adv. Mater.* **2020**, *32*, 1906548.

(10) Ji, L.; Rao, M.; Zheng, H.; Zhang, L.; Li, Y.; Duan, W.; Guo, J.; Cairns, E. J.; Zhang, Y. Graphene oxide as a sulfur immobilizer in high performance lithium/sulfur cells. *J. Am. Chem. Soc.* **2011**, *133*, 18522−18525.

(11) Liu, Y.; Zhou, G.; Liu, K.; Cui, Y. Design of Complex Nanomaterials for Energy Storage: Past Success and Future Opportunity. *Acc. Chem. Res.* **2017**, *50*, 2895−2905.

(12) Fang, R.; Zhao, S.; Hou, P.; Cheng, M.; Wang, S.; Cheng, H. M.; Liu, C.; Li, F. 3D interconnected electrode materials with ultrahigh areal sulfur loading for Li−S batteries. *Adv. Mater.* **2016**, *28*, 3374−3382.

(13) Urbonaite, S.; Poux, T.; Novák, P. Progress towards commercially viable Li−S battery cells. *Adv. Energy Mater.* **2015**, *5*, 1500118.

(14) Jeong, Y. C.; Kim, J. H.; Nam, S.; Park, C. R.; Yang, S. J. Rational Design of Nanostructured Functional Interlayer/Separator for Advanced Li−S Batteries. *Adv. Funct. Mater.* **2018**, *28*, 1707411.

(15) Yin, Y. X.; Xin, S.; Guo, Y. G.; Wan, L. J. Lithium-sulfur batteries: electrochemistry, materials, and prospects. *Angew. Chem., Int. Ed.* **2013**, *52*, 13186−13200.

(16) Yang, X.-F.; Wang, A.; Qiao, B.; Li, J.; Liu, J.; Zhang, T. Single-atom catalysts: a new frontier in heterogeneous catalysis. *Acc. Chem. Res.* **2013**, *46*, 1740−1748.

(17) Chen, Y.; Ji, S.; Chen, C.; Peng, Q.; Wang, D.; Li, Y. Single-atom catalysts: synthetic strategies and electrochemical applications. *Joule* **2018**, *2*, 1242−1264.

(18) Guan, C.; Sumboja, A.; Wu, H.; Ren, W.; Liu, X.; Zhang, H.; Liu, Z.; Cheng, C.; Pennycook, S. J.; Wang, J. Hollow Co3 O4 Nanosphere Embedded in Carbon Arrays for Stable and Flexible Solid-State Zinc-Air Batteries. *Adv. Mater.* **2017**, *29*, 1704117.

(19) Wang, X. X.; Cullen, D. A.; Pan, Y. T.; Hwang, S.; Wang, M.; Feng, Z.; Wang, J.; Engelhard, M. H.; Zhang, H.; He, Y.; et al. Nitrogen-coordinated single cobalt atom catalysts for oxygen reduction in proton exchange membrane fuel cells. *Adv. Mater.* **2018**, *30*, 1706758.

(20) Chen, M.; He, Y.; Spendelow, J. S.; Wu, G. Atomically Dispersed Metal Catalysts for Oxygen Reduction. *ACS Energy Letters* **2019**, *4*, 1619−1633.

(21) Zhang, H.; Hwang, S.; Wang, M.; Feng, Z.; Karakalos, S.; Luo, L.; Qiao, Z.; Xie, X.; Wang, C.; Su, D.; Shao, Y.; Wu, G. Single Atomic Iron Catalysts for Oxygen Reduction in Acidic Media: Particle Size Control and Thermal Activation. *J. Am. Chem. Soc.* **2017**, *139*, 14143−14149.

(22) Lin, Y.; Liu, P.; Velasco, E.; Yao, G.; Tian, Z.; Zhang, L.; Chen, L. Fabricating Single-Atom Catalysts from Chelating Metal in Open Frameworks. *Adv. Mater.* **2019**, *31*, 1.

(23) Chen, Y.; Ji, S.; Wang, Y.; Dong, J.; Chen, W.; Li, Z.; Shen, R.; Zheng, L.; Zhuang, Z.; Wang, D.; Li, Y. Isolated Single Iron Atoms Anchored on N-Doped Porous Carbon as an Efficient Electrocatalyst for the Oxygen Reduction Reaction. *Angew. Chem., Int. Ed.* **2017**, *56*, 6937−6941.

(24) Jiao, L.; Wan, G.; Zhang, R.; Zhou, H.; Yu, S. H.; Jiang, H. L. From Metal−Organic Frameworks to Single-Atom Fe Implanted N-doped Porous Carbons: Efficient Oxygen Reduction in Both Alkaline and Acidic Media. *Angew. Chem., Int. Ed.* **2018**, *57*, 8525−8529.

(25) Zitolo, A.; Goellner, V.; Armel, V.; Sougrati, M. T.; Mineva, T.; Stievano, L.; Fonda, E.; Jaouen, F. Identification of catalytic sites for oxygen reduction in iron- and nitrogen-doped graphene materials. *Nat. Mater.* **2015**, *14*, 937−942.

(26) Zhao, L.; Zhang, Y.; Huang, L. B.; Liu, X. Z.; Zhang, Q. H.; He, C.; Wu, Z. Y.; Zhang, L. J.; Wu, J.; Yang, W.; Gu, L.; Hu, J. S.; Wan, L.

J. Cascade anchoring strategy for general mass production of high-loading single-atomic metal-nitrogen catalysts. *Nat. Commun.* **2019**, *10*, 1278.
(27) Lu, C.; Yang, Y.; Chen, X. Ultrathin conductive graphitic carbon nitride assembly through van der Waals epitaxy toward high energy-density flexible supercapacitors. *Nano Lett.* **2019**, *19*, 4103−4111.
(28) Xu, J.; Xu, F.; Qian, M.; Xu, F.; Hong, Z.; Huang, F. Conductive Carbon Nitride for Excellent Energy Storage. *Adv. Mater.* **2017**, *29*, 1701674.
(29) Wang, X.; Maeda, K.; Thomas, A.; Takanabe, K.; Xin, G.; Carlsson, J. M.; Domen, K.; Antonietti, M. A metal-free polymeric photocatalyst for hydrogen production from water under visible light. *Nat. Mater.* **2009**, *8*, 76−80.
(30) Lu, C.; Wang, D.; Zhao, J.; Han, S.; Chen, W. A Continuous Carbon Nitride Polyhedron Assembly for High-Performance Flexible Supercapacitors. *Adv. Funct. Mater.* **2017**, *27*, 1606219.
(31) Liu, J.; Zhang, L.; Wu, H. B.; Lin, J.; Shen, Z.; Lou, X. W. High-performance flexible asymmetric supercapacitors based on a new graphene foam/carbon nanotube hybrid film. *Energy Environ. Sci.* **2014**, *7*, 3709−3719.
(32) Peng, P.; Shi, L.; Huo, F.; Mi, C.; Wu, X.; Zhang, S.; Xiang, Z. A pyrolysis-free path toward superiorly catalytic nitrogen-coordinated single atom. *Sci. Adv.* **2019**, *5*, No. eaaw2322.
(33) Han, A.; Wang, B.; Kumar, A.; Qin, Y.; Jin, J.; Wang, X.; Yang, C.; Dong, B.; Jia, Y.; Liu, J.; Sun, X. Recent Advances for MOF-Derived Carbon-Supported Single-Atom Catalysts. *Small Methods* **2019**, *3*, 1800471.
(34) Xue, Y.; Huang, B.; Yi, Y.; Guo, Y.; Zuo, Z.; Li, Y.; Jia, Z.; Liu, H.; Li, Y. Anchoring zero valence single atoms of nickel and iron on graphdiyne for hydrogen evolution. *Nat. Commun.* **2018**, *9*, 1460.
(35) Liu, J.; Li, W.; Duan, L.; Li, X.; Ji, L.; Geng, Z.; Huang, K.; Lu, L.; Zhou, L.; Liu, Z.; Chen, W.; Liu, L.; Feng, S.; Zhang, Y. A Graphene-like Oxygenated Carbon Nitride Material for Improved Cycle-Life Lithium/Sulfur Batteries. *Nano Lett.* **2015**, *15*, 5137−5142.
(36) Wu, Y.; Zhu, X.; Li, P.; Zhang, T.; Li, M.; Deng, J.; Huang, Y.; Ding, P.; Wang, S.; Zhang, R.; Lu, J.; Lu, G.; Li, Y.; Li, Y. Ultradispersed WxC nanoparticles enable fast polysulfide interconversion for high-performance Li-S batteries. *Nano Energy* **2019**, *59*, 636−643.
(37) Yuan, H.; Chen, X.; Zhou, G.; Zhang, W.; Luo, J.; Huang, H.; Gan, Y.; Liang, C.; Xia, Y.; Zhang, J.; Wang, J.; Tao, X. Efficient Activation of Li2S by Transition Metal Phosphides Nanoparticles for Highly Stable Lithium−Sulfur Batteries. *ACS Energy Lett.* **2017**, *2*, 1711−1719.
(38) Tao, X.; Wang, J.; Liu, C.; Wang, H.; Yao, H.; Zheng, G.; Seh, Z. W.; Cai, Q.; Li, W.; Zhou, G.; Zu, C.; Cui, Y. Balancing surface adsorption and diffusion of lithium-polysulfides on nonconductive oxides for lithium−sulfur battery design. *Nat. Commun.* **2016**, *7*, 11203.
(39) Klein, M. J.; Dolocan, A.; Zu, C.; Manthiram, A. An Effective Lithium Sulfide Encapsulation Strategy for Stable Lithium−Sulfur Batteries. *Adv. Energy Mater.* **2017**, *7*, 1701122.
(40) Sun, Y.; Lee, H.-W.; Seh, Z. W.; Zheng, G.; Sun, J.; Li, Y.; Cui, Y. Lithium Sulfide/Metal Nanocomposite as a High-Capacity Cathode Prelithiation Material. *Adv. Energy Mater.* **2016**, *6*, 1600154.
(41) Hwa, Y.; Zhao, J.; Cairns, E. J. Lithium Sulfide (Li2S)/Graphene Oxide Nanospheres with Conformal Carbon Coating as a High-Rate, Long-Life Cathode for Li/S Cells. *Nano Lett.* **2015**, *15*, 3479−3486.
(42) Ansari, Y.; Zhang, S.; Wen, B.; Fan, F.; Chiang, Y.-M. Stabilizing Li−S Battery Through Multilayer Encapsulation of Sulfur. *Adv. Energy Mater.* **2019**, *9*, 1802213.
(43) Hua, W.; Yang, Z.; Nie, H.; Li, Z.; Yang, J.; Guo, Z.; Ruan, C.; Chen, X. a.; Huang, S. Polysulfide-scission reagents for the suppression of the shuttle effect in lithium−sulfur batteries. *ACS Nano* **2017**, *11*, 2209−2218.
(44) Yeon, J. S.; Yun, S.; Park, J. M.; Park, H. S. Surface-Modified Sulfur Nanorods Immobilized on Radially Assembled Open-Porous Graphene Microspheres for Lithium-Sulfur Batteries. *ACS Nano* **2019**, *13*, 5163−5171.
(45) Tian, W.; Xi, B.; Feng, Z.; Li, H.; Feng, J.; Xiong, S. Sulfiphilic Few-Layered MoSe2 Nanoflakes Decorated rGO as a Highly Efficient Sulfur Host for Lithium-Sulfur Batteries. *Adv. Energy Mater.* **2019**, *9*, 1901896.
(46) Li, Z.; Zhang, J.; Lou, X. W. Hollow carbon nanofibers filled with MnO2 nanosheets as efficient sulfur hosts for lithium−sulfur batteries. *Angew. Chem., Int. Ed.* **2015**, *54*, 12886−12890.
(47) Peng, H. J.; Zhang, G.; Chen, X.; Zhang, Z. W.; Xu, W. T.; Huang, J. Q.; Zhang, Q. Enhanced electrochemical kinetics on conductive polar mediators for lithium−sulfur batteries. *Angew. Chem., Int. Ed.* **2016**, *55*, 12990−12995.
(48) Du, Z.; Chen, X.; Hu, W.; Chuang, C.; Xie, S.; Hu, A.; Yan, W.; Kong, X.; Wu, X.; Ji, H.; Wan, L. J. Cobalt in Nitrogen-Doped Graphene as Single-Atom Catalyst for High-Sulfur Content Lithium-Sulfur Batteries. *J. Am. Chem. Soc.* **2019**, *141*, 3977−3985.
(49) Wang, T.; Zhu, J.; Wei, Z.; Yang, H.; Ma, Z.; Ma, R.; Zhou, J.; Yang, Y.; Peng, L.; Fei, H.; Lu, B.; Duan, X. Bacteria Derived Biological Carbon Building Robust Li-S Batteries. *Nano Lett.* **2019**, *19*, 4384−4390.
(50) Wang, Y.; Zhang, R.; Chen, J.; Wu, H.; Lu, S.; Wang, K.; Li, H.; Harris, C. J.; Xi, K.; Kumar, R. V.; Ding, S. Enhancing Catalytic Activity of Titanium Oxide in Lithium−Sulfur Batteries by Band Engineering. *Adv. Energy Mater.* **2019**, *9*, 1900953.
(51) Fang, D.; Wang, Y.; Liu, X.; Yu, J.; Qian, C.; Chen, S.; Wang, X.; Zhang, S. Spider-Web-Inspired Nanocomposite Modified Separator: Structural and Chemical Cooperativity Inhibiting the Shuttle Effect in Li-S Batteries. *ACS Nano* **2019**, *13*, 1563−1573.
(52) Zhou, G.; Tian, H.; Jin, Y.; Tao, X.; Liu, B.; Zhang, R.; Seh, Z. W.; Zhuo, D.; Liu, Y.; Sun, J.; Zhao, J.; Zu, C.; Wu, D. S.; Zhang, Q.; Cui, Y. Catalytic oxidation of Li2S on the surface of metal sulfides for Li-S batteries. *Proc. Natl. Acad. Sci. U. S. A.* **2017**, *114*, 840−845.
(53) Xie, Y.; Meng, Z.; Cai, T.; Han, W.-Q. Effect of Boron-Doping on the Graphene Aerogel Used as Cathode for the Lithium−Sulfur Battery. *ACS Appl. Mater. Interfaces* **2015**, *7*, 25202−25210.
(54) Xu, J.; Su, D.; Zhang, W.; Bao, W.; Wang, G. A nitrogen−sulfur co-doped porous graphene matrix as a sulfur immobilizer for high performance lithium−sulfur batteries. *J. Mater. Chem. A* **2016**, *4*, 17381−17393.
(55) Song, J.; Xu, T.; Gordin, M. L.; Zhu, P.; Lv, D.; Jiang, Y.-B.; Chen, Y.; Duan, Y.; Wang, D. Nitrogen-Doped Mesoporous Carbon Promoted Chemical Adsorption of Sulfur and Fabrication of High-Areal-Capacity Sulfur Cathode with Exceptional Cycling Stability for Lithium-Sulfur Batteries. *Adv. Funct. Mater.* **2014**, *24*, 1243−1250.
(56) Zhao, Y.; Wu, W.; Li, J.; Xu, Z.; Guan, L. Encapsulating MWNTs into Hollow Porous Carbon Nanotubes: A Tube-in-Tube Carbon Nanostructure for High-Performance Lithium-Sulfur Batteries. *Adv. Mater.* **2014**, *26*, 5113−5118.
(57) Dong, Y.; Lu, P.; Shi, H.; Qin, J.; Chen, J.; Ren, W.; Cheng, H.-M.; Wu, Z.-S. 2D hierarchical yolk-shell heterostructures as advanced host-interlayer integrated electrode for enhanced Li-S batteries. *J. Energy Chem.* **2019**, *36*, 64−73.
(58) Jiang, J.; Fan, Q.; Chou, S.; Guo, Z.; Konstantinov, K.; Liu, H.; Wang, J. Li2S-Based Li-Ion Sulfur Batteries: Progress and Prospects. *Small* **2019**, 1903934.
(59) Liu, Y.; Li, X.; Liu, Y.; Kou, W.; Shen, W.; He, G. Promoting opposite diffusion and efficient conversion of polysulfides in "Trap" Fe C-Doped asymmetric porous membranes as integrated electrodes. *Chem. Eng. J.* **2020**, *382*, 122858.
(60) Zheng, C.; Niu, S.; Lv, W.; Zhou, G.; Li, J.; Fan, S.; Deng, Y.; Pan, Z.; Li, B.; Kang, F.; Yang, Q.-H. Propelling polysulfides transformation for high-rate and long-life lithium−sulfur batteries. *Nano Energy* **2017**, *33*, 306−312.
(61) Tang, C.; Zhang, Q.; Zhao, M.-Q.; Huang, J.-Q.; Cheng, X.-B.; Tian, G.-L.; Peng, H.-J.; Wei, F. Nitrogen-Doped Aligned Carbon Nanotube/Graphene Sandwiches: Facile Catalytic Growth on Bifunctional Natural Catalysts and Their Applications as Scaffolds for High-Rate Lithium-Sulfur Batteries. *Adv. Mater.* **2014**, *26*, 6100−6105.

https://dx.doi.org/10.1021/acs.nanolett.0c02167
Nano Lett. 2020, 20, 5522−5530

(62) Li, L.; Chen, L.; Mukherjee, S.; Gao, J.; Sun, H.; Liu, Z.; Ma, X.; Gupta, T.; Singh, C. V.; Ren, W.; Cheng, H.-M.; Koratkar, N. Phosphorene as a Polysulfide Immobilizer and Catalyst in High-Performance Lithium−Sulfur Batteries. *Adv. Mater.* **2017**, *29*, 1602734.

https://dx.doi.org/10.1021/acs.nanolett.0c02167
Nano Lett. 2020, 20, 5522−5530